Single-mode quantum-cascade lasers with variable etching depth of grating slits

© A.V. Babichev[1], N.Yu. Kharin[2], E.S. Kolodeznyi[1], D.S. Papylev[1], G.V. Voznyuk[3], M.I. Mitrofanov[3,4], A.G. Gladyshev[1], S.O. Slipchenko[3], A.V. Lyutetsky[3], V.P. Evtikhiev[3], V.Yu. Panevin[2], L.Ya. Karachinsky[1], I.I. Novikov[1], N.A. Pikhtin[3], A.Yu. Egorov[1]

[1] ITMO University,
197101 St. Petersburg, Russia
[2] Peter the Great Saint-Petersburg Polytechnic University,
195251 St. Petersburg, Russia
[3] Ioffe Institute,
194021 St. Petersburg, Russia
[4] Submicron Heterostructures for Microelectronics, Research and Engineering Center,
Russian Academy of Sciences,
194021 St. Petersburg, Russia

E-mail: a.babichev@mail.ioffe.ru; Researcher ID: F-6479-2015

Received March 17, 2025
Revised March 31, 2025
Accepted April 10, 2025

The results of the study of surface-emitting quantumcascade lasers with a ring cavity radius of 284 μm were presented. The use of a grating with a variable etching depth (up to 4.6 μm) provided a single-mode lasing at a wavelength of 7.42 and 7.66 μm at a temperature of 85 and 293 K. The maximum side-mode suppression ratio was 23 dB at 293 K. The characteristic temperature T_0 was 166 K.

Keywords: quantum-cascade laser, single-mode lasing, indium phosphide, direct ion-beam lithography, grating.

DOI: 10.61011/SC.2025.01.61071.7698

1. Introduction

Quantum-cascade lasers (QCL) with distributed feedback (DFB) are traditionally used for gas analysis [1]. Diode laser absorption spectroscopy systems based on (Herriott) multi-pass cells are used to reduce the gas detection threshold (to 10^{-8} [2,3]). Employment of these spectroscopy systems is associated with the need to implement low-divergence QCL [4].

Ring cavity design provides a 20 times lower radiation divergence than that of stripe-geometry QCL [4]. Additional radiation focusing is possible when abrupt or smooth phase shift is implemented [5,6] by employing metasurfaces [4] and diffraction grating with a variable groove etching depth [7].

This work shows results of formation and study of quantum-cascade lasers with selective ring cavity where diffraction grating grooves were etched by the direct ion lithography method.

2. Experimental samples

A quantum-cascade laser heterostructure was grown by the molecular-beam epitaxy on a heavily doped InP substrate with the (100) crystal-lattice orientation. A 35-period active region configuration described in [8] was used to increase the laser voltage efficiency. This configuration with one-phonon depletion of the lower laser level followed by charge carrier emission through a mini-band has demonstrated a record-breaking optical output power (3.6 W for laser with a contact width of 20 μm and cavity length of 3 mm [8]) among the active regions including 35 periods in an unstressed heteropair cascade. Despite the fact that a higher maximum optical output power (4.4 W) was previously demonstrated for lasers based on the active region configuration with two-phonon lower level depletion [9], the laser wall-plug efficiency (WPE) is 1.5 times lower (3.8 %) than that of the configuration discussed in [8] (5.6 % at the current pumping level of 6 A). Indium phosphide layers were used as the waveguide plates. The total thickness of the bottom and top waveguide plates was 3.5 μm and 4.2 μm. Additional 250 nm $In_{0.53}Ga_{0.47}As$ layers limited the active region.

Ring cavity with a mean radius of 284 μm and near-surface width of 19 μm was formed by means of wet etching of a double mesastructure to a depth of $\sim 11\,\mu$m. After formation of SiO_2-based insulation and opening of a window in the insulation, top contact metallization (Ti/Au) was sputtered. Bottom metallization was formed after substrate thinning. Laser was mounted on a copper heatsink.

Diffraction grating profile was formed using the direct (maskless) ion lithography method. This method may be used together with using the gray-scale lithography for formation of a diffraction grating with a variable etching depth. Diffraction grating formation method was chosen considering the following factors:

1) advantage of the electron-beam gray-scale lithography compared with the laser gray-scale lithography is in smooth

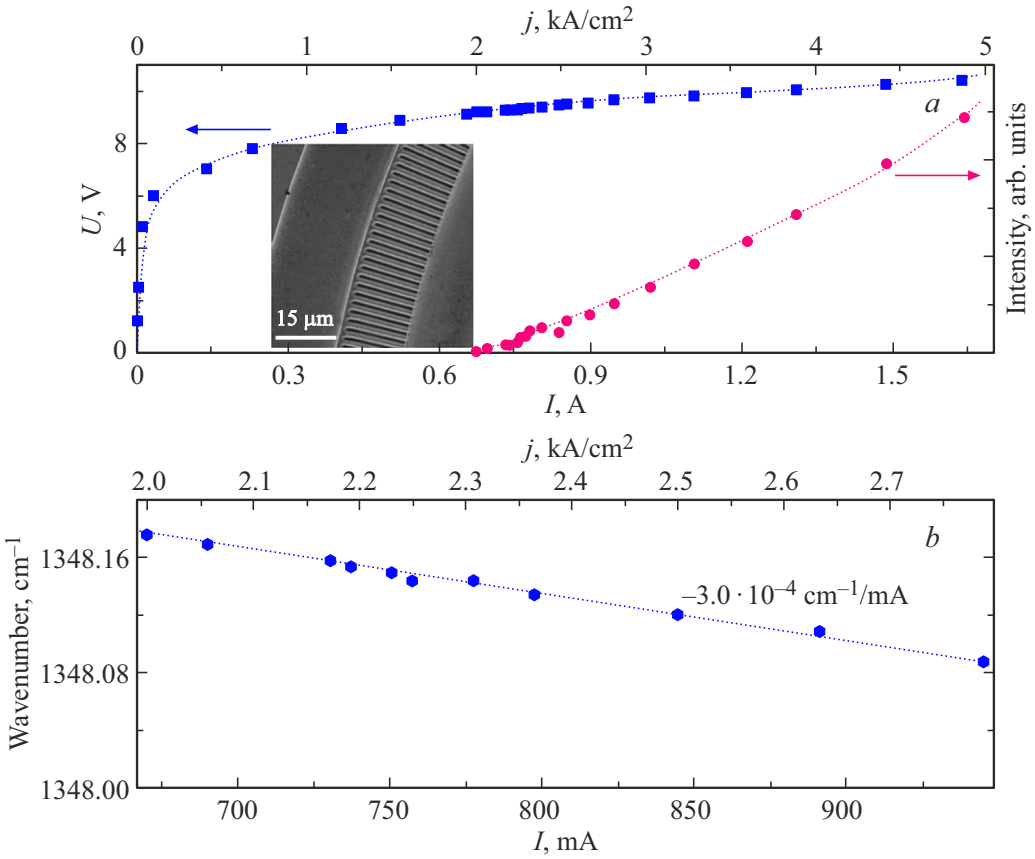

Figure 1. Volt-ampere and watt-ampere curves of selective ring cavity QCL (*a*). The inset shows a scanning electron microscopy image. Single-frequency lasing line shift with an increase in the current pumping level (*b*). Sample temperature is 85 K.

resist exposure variation capability and submicronic resolution of the formed profile [10];

2) electron-beam gray-scale lithography is used because special glass is needed, transparency of which depends on the focused electron beam pumping level (high energy beam sensitive glass, HEBS);

3) after development of the resist exposed by the gray-scale lithography method, a 3D profile is formed in the layers of the resist that serves as a mask. During „dry" etching [11–14] in methane-containing and chlorine-containing plasma, this profile is translated into the top waveguide plate layers. Thus, the main disadvantage of the gray-scale lithography method is a small difference between the minimum and maximum etching depths defined by the resist thickness ($\leq 1\,\mu$m);

4) maskless ion lithography has no any fundamental limit for diffraction grating groove etching depth.

Direct ion lithography method was used to form 753 2-nd order diffraction grating grooves on the ring cavity circumference. Groove period (Λ) and groove width were 2.37 μm and 16 μm, pulse period-duration ratio was 50 %. Minimum etching depth of the diffraction grating grooves was equal to the top metallization thickness ($\sim 0.6\,\mu$m). Maximum etching depth was increased for this waveguide design up to 4.55 μm (regardless of the top metallization thickness) compared with 3.8 μm deposited previously [15]. Focused ion-beam etching of grooves was performed by the operating current of 2.1 nA with ion energy of 20 keV. Groove exposure time was 16 s. Full ion dose for various grooves varied in the range of $5.25 \cdot 10^{17} - 1.7 \cdot 10^{18}$ cm^{-2}. Scanning electron microscopy image of the selective ring cavity is shown in the inset in Figure 1.

Lasing spectra were recorded by the Bruker Vertex 80v Fourier spectrometer in the step-scan mode. Spectral resolution was 0.2 cm^{-1}. Pulse duration and repetition rate were 150 ns and 10 kHz. Laser properties were measured at 85 K and 293 K with the sample placed in a cryostat with temperature stabilization.

3. Results and discussion

Dependence of integral radiation intensity on the current pumping level together with current-voltage curve at 85 K are shown in Figure 1, *a*. Threshold current (I_{th}) was 0.67 A. Active region configuration described previously in [8] was used to reduce the threshold voltage from 13.5 V [15] to 9.2 V due to the reduction of the number of periods in the cascade and change of the bottom level and injector depletion scheme. Taking into account the number of periods in the cascade, low defect voltage at lasing

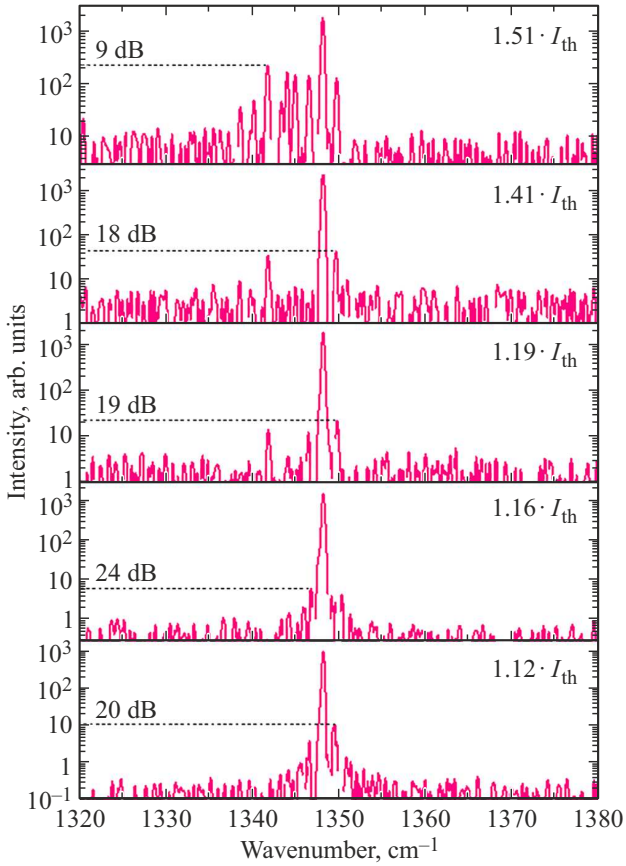

Figure 2. Single-frequency lasing spectra at various current pumping levels (semilogarithmic scale). Sample temperature is 85 K.

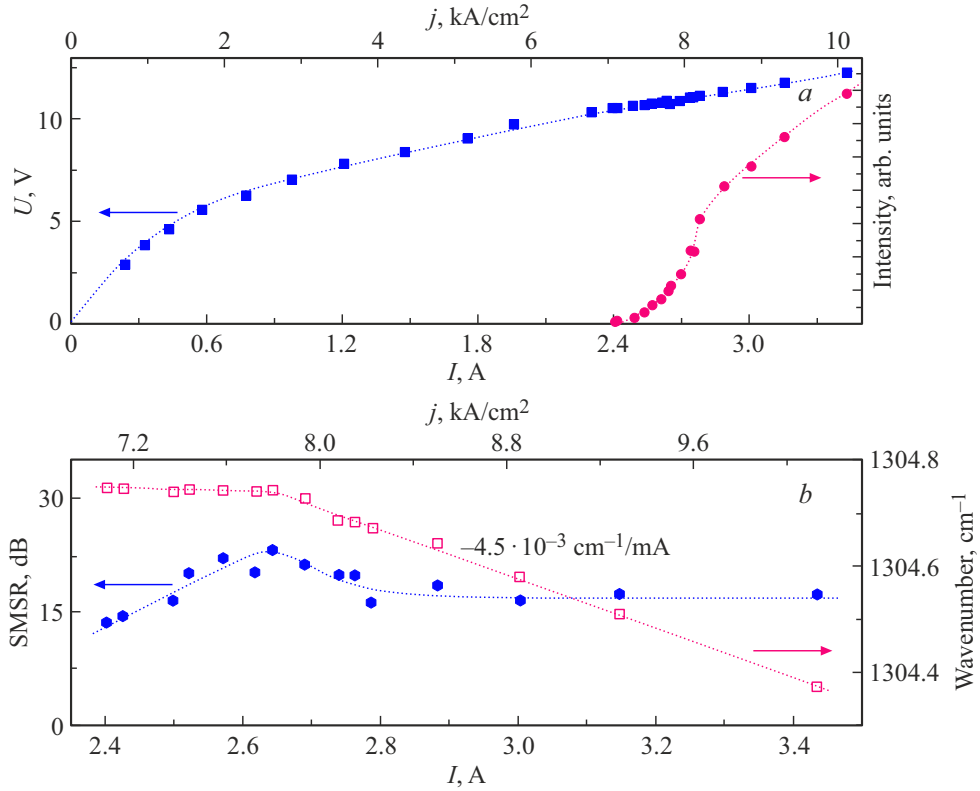

Figure 3. Volt-ampere and watt-ampere curves of selective ring cavity QCL (a). Side-mode suppression ratio and position of the single-frequency lasing line from the current pumping level (b). Sample temperature is 293 K.

threshold (95 meV) was demonstrated, which somehow exceeds the minimum value (90 meV [16]) for short-injector configurations. Threshold current density j_{th} for the selected ring cavity QCL under study was 2.0 kA/cm^2. Voltage corresponding to the cascade period misalignment [17] was equal to 12.7 V, which corresponded to the defect voltage of 196 meV. Thus, saturation of the watt-ampere characteristic is observed when the threshold current is exceeded fivefold.

Selective ring cavity lasing spectra measured at 85 K are shown in Figure 2. Mode hop free single-frequency lasing at 7.42 μm is demonstrated. Side-mode suppression ratio (SMSR) near the lasing threshold was 20 dB. Lasing threshold exceeded by 16 % provided an increase in SMSR to 24 dB. SMSR at the level of 18–19 dB is demonstrated up to $1.41 \cdot I_{th}$. Lasing threshold exceeded by 50 % leads to switching to a multimode lasing regime. Lasing spectrum is represented by 8 radial modes. Further increase of the current pumping level (to $2.43 \cdot I_{th}$) leads to the growth of lasing line intensity in the wavelength range of 7.57–7.69 μm and lasing line intensity suppression near 7.44 μm. Single-frequency lasing line shift was estimated with the increase in the current pumping density level (see Figure 1, *b*) which was -0.1 cm/kA.

Single-frequency generation (at 7.66 μm) at room temperature was demonstrated. Dependence of the integral radiation intensity on the current pumping level together with current-voltage curve at 293 K are shown in Figure 3, *a*. Threshold current and current density corresponding to 9.2 V were 2.4 A and 7 kA/cm^2, respectively. Estimated characteristic temperature T_0 is 166 K. Lasing spectra at 293 K are shown in Figure 4. Spectrum near the threshold is represented by two radial modes with SMSR equal to 14 dB. Increase in the current pumping level to 2.64 A leads to consecutive increase in SMSR to 23 dB. Further increase in the current pumping level to 3.4 A leads to a decrease in SMSR to 17 dB. Figure 3, *b* shows the lasing line position from the pumping level. Increase in current from 2.6 A to 3.4 A induces a long-wavelength shift of the lasing line position $\sim 0.4\,\text{cm}^{-1}$. Current and pumping current density shift rates of the lasing line position were $-4.5 \cdot 10^{-3}\,\text{cm}^{-1}/\text{mA}$ and $-0.16\,\text{cm}^{-1}/\text{kA}$, respectively. This value exceeds the previously shown value for single-frequency lasers (-0.1 cm/kA [15,18]), which is caused by the differences in laser configuration. Note that a decrease in SMSR with the pumping level growth is correlated with the starting time of the lasing line position shift induced by laser warming up (see Figure 3, *b*). Taking into account the temperature shift of the lasing line position that was $-0.209\,\text{cm}^{-1}/\text{K}$ for the cavity design under study, which correlates with previous findings [19], laser warming up was estimated It is shown that an increase in the current pumping level up to 1.5 threshold values causes a rise of laser temperature by maximum 2 K.

Radial mode order (m) was estimated to determine the radiation divergence in the far-field intensity distribution.

At pumping currents up to $1.07 \cdot I_{th}$, intermode spacing $d\nu$ is $\sim 1.66\,\text{cm}^{-1}$. Consequently, the effective refractive index $n_{eff} = 1/(2\pi R_{out} d\nu) = 3.27$, where R_{out} is the external ring cavity radius [13]. m may be evaluated using the following expression [13]: $m = 2\pi R_{out}(n_{eff}/\lambda - 1/\Lambda)$, where λ is the spectral position of the lasing line. It is shown that lasing corresponds to the 8th order mode. Taking into account expression [13]: $\sin(2\Theta) = (n + m/2)\lambda/R_{out}$, angular position of the first and second maxima in the far-field intensity distribution was estimated to evaluate the far-field distribution FWHM ($\sim 2^\circ$).

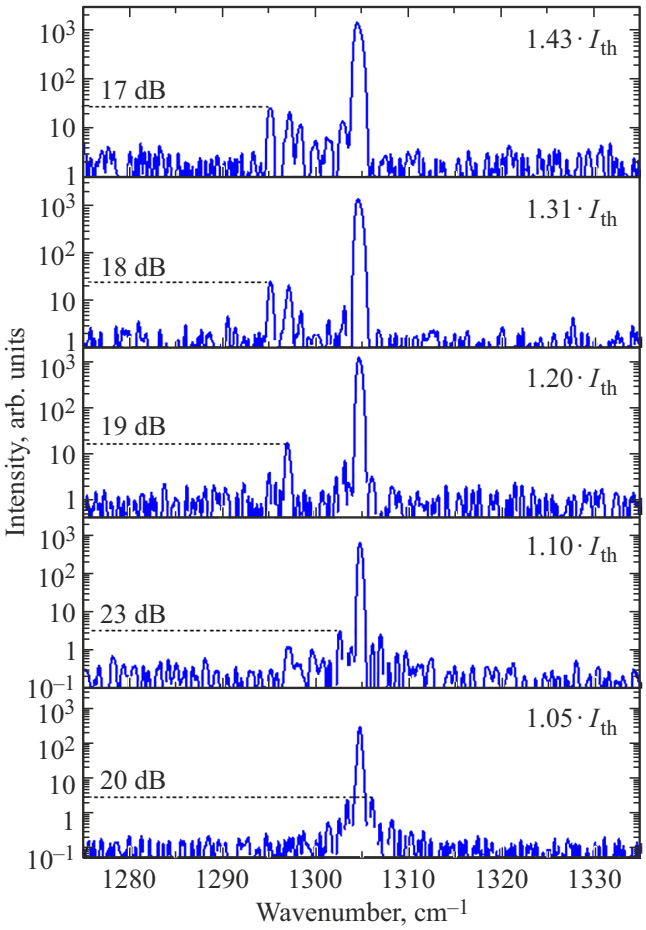

Figure 4. Single-frequency lasing spectra at various current pumping levels (semilogarithmic scale). Sample temperature is 293 K.

4. Conclusion

The first results of implementing single-frequency quantum-cascade lasers with variable etching depth of diffraction grating grooves operating at room temperature (293 K) are shown. Active region configuration with one-phonon depletion of the bottom laser level followed by charge carrier emission through a mini-band was used to increase the laser efficiency. At 85 K, low threshold current density (2 kA/cm^2) was implemented for a configuration with an increased (up to 4.6 μm) diffraction grating groove etching depth. Single-frequency lasing mode at 7.42 μm was demonstrated. Maximum SMSR was 24 dB. Temperature

rise to 293 K made it possible to implement single-frequency lasing at 7.66 μm with the maximum SMSR of 23 dB. Threshold current density was 7 kA/cm^2. Increase in the threshold value by 43 % led to a lasing wavelength shift corresponding to laser warming up of ~ 2 K. Intermode spacing in lasing spectra was used to estimate radiation divergence in the far-field intensity distribution that was equal to $\sim 2^\circ$.

Funding

The study of laser characteristics performed by the authors from the ITMO University was supported financially by grant No. 20-79-10285−P issued by the Russian Science Foundation, https://rscf.ru/project/20-79-10285/.

Conflict of interest

The authors declare that they have no conflict of interest.

References

[1] D. Hofstetter, M. Beck, J. Faist, M. Nägele, M.W. Sigrist. Optics Lett., **26** (12), 887 (2001).
[2] C. Wang, P. Sahay. Sensors, **9** (10), 8230 (2009).
[3] P.I.Abramov, E.V.Kuznetsov, L.A.Skvortsov, M.I.Skvortsov. ZhPS, **1** (5), 2019 (2023). (in Russian).
[4] R. Szedlak, C. Schwarzer, T. Zederbauer, H. Detz, A. Maxwell Andrews, W. Schrenk, G. Strasser. Appl. Phys. Lett., **104** (15), 151105 (2014).
[5] R. Szedlak, M. Holzbauer, D. MacFarland, T. Zederbauer, H. Detz, A.M. Andrews, C. Schwarzer, W. Schrenk, G. Strasser. Sci. Rep., **5** (1), 16668 (2015).
[6] R. Szedlak, T. Hisch, B. Schwarz, M. Holzbauer, D. MacFarland, T. Zederbauer, H. Detz, A.M. Andrews, W. Schrenk, S. Rotter, G. Strasser. Sci. Rep., **8** (1), 7998 (2018).
[7] P.N. Figueiredo, A. Muraviev, R.E. Peale. Proc. SPIE, **9466**, 946602 (2015).
[8] A.V. Babichev, E.S. kolodezny, D.A. Mikhailov, V.V. Dyudelev, A.G. Gladyshev, S.O. Slipchenko, A.V. Lutetsky, L.Ya. Karachinsky, I.I. Novikov, G.S. Sokolovsky, N.A. Pikhtin, A.Yu. Egorov. Pis'ma ZhTF, **50** (16), 18 (2024). (in Russian).
[9] A.V. Babichev, D.A. Pashnev, A.G. Gladyshev, A.S. Kurochkin, E.S. Kolodeznyi, L.Ya. Karachinsky, I.I. Novikov, D.V. Denisov, L. Boulley, D.A. Firsov, L.E. Vorobjev, N.A. Pikhtin, A. Bousseksou, A.Yu. Egorov. Techn. Phys. Lett., **45** (11), 1136 (2019).
[10] C. Schuster, M. Heinrich, A. Voigt, A. Zanzal, P. Reynolds, S. DeMoor, G. Ekindorf, A. Schleunitz, G. Gruetzner. Proc. SPIE, **12956**, 129560H (2024).
[11] G. Marschick, J. Pelini, T. Gabbrielli, F. Cappelli, R. Weih, H. Knötig, J. Koeth, S. Höfling, P. De Natale, G. Strasser, S. Borri, B. Hinkov. ACS Photonics, **11** (2), 395 (2024).
[12] G. Marschick, S. Isceri, R. Szedlak, H. Moser, J.P. Waclawek, E. Arigliani, R. Weih, W. Schrenk, G. Strasser, B. Hinkov, A. Maxwell A.B. Lendl, B. Schwarz. APL Photonics, **9** (10), 100806 (2024).
[13] Y. Bai, S. Tsao, N. Bandyopadhyay, S. Slivken, Q.Y. Lu, D. Caffey, M. Pushkarsky, T. Day, M. Razeghi. Appl. Phys. Lett., **99** (26), 261104 (2011).
[14] M. Shahmohammadi, F. Kapsalidis, M.J. Süess, E. Gini, M. Beck, M. Hundt, B. Tuzson, L. Emmenegger, J. Faist. Semicond. Sci. Technol., **34** (8), 083001 (2019).
[15] A.V. Babichev, N.Yu. Kharin, E.S. Kolodezny, D.A. Mikhailov, G.V. Voznyuk, M.I. Mitrofanov, V.V. Dyudelev, A.G. Gladyshev, S.O. Slipchenko, A.V. Lyutetsky, V.P. Yevtikhiev, V.Yu. Panevin, L.Ya. Karachinsky, I.I. Novikov, G.S. Sokolovsky, N.A. Pikhtin, A.Yu. Yegorov. PZhTF **11**, 52 (2025). (in Russian).
[16] W. Zhou, Q.-Y. Lu, D.-H. Wu, S. Slivken, M. Razeghi. Opt. Express, **27** (11), 15776 (2019).
[17] A. Lyakh, R. Maulini, A. Tsekoun, R. Go, C.K.N. Patel. Opt. Express, **20** (22), 24272 (2012).
[18] A.V. Babichev, E.S. Kolodeznyi, A.G. Gladyshev, D.V. Denisov, N.Yu. Kharin, A.D. Petruk, V.Yu. Panevin, S.O. Slipchenko, A.V. Lyutetskii, L.Ya. Karachinsky, I.I. Novikov, N.A. Pikhtin, A.Yu. Egorov. Techn. Phys. Lett., **48** (3), 69 (2022).
[19] D.H. Wu, M. Razeghi. APL Materials, **5** (3), 035505 (2017).

Translated by E.Ilinskaya